

Potential Energy Landscapes for the 2D XY Model: Minima, Transition States and Pathways

Dhagash Mehta,^{1,*} Ciaran Hughes,^{2,†} Mario Schröck,^{3,‡} and David J. Wales^{4,§}

¹*Dept of Mathematics, North Carolina State University, Raleigh, NC 27695, USA.*

²*The Department of Applied Mathematics and Theoretical Physics,
The University of Cambridge, Clarkson Road, Cambridge CB3 0EH, UK.*

³*Institut für Physik, FB Theoretische Physik, Universität Graz, 8010 Graz, Austria.*

⁴*University Chemical Laboratories, Lensfield Road, Cambridge CB2 1EW, UK.*

Abstract

We describe a numerical study of the potential energy landscape for the two-dimensional XY model (with no disorder), considering up to 100 spins and CPU and GPU implementations of local optimization, focusing on minima and saddles of index one (transition states). We examine both periodic and anti-periodic boundary conditions, and show that the number of stationary points located increases exponentially with increasing lattice size. The corresponding disconnectivity graphs exhibit funneled landscapes; the global minima are readily located because they exhibit relatively large basins of attraction compared to the higher energy minima as the lattice size increases.

* dbmehta@ncsu.edu

† ch558@cam.ac.uk

‡ mario.schroeck@uni-graz.at

§ dw34@cam.ac.uk

I. INTRODUCTION

Stationary points of a potential energy function, defined as configurations where the gradient vanishes, play a key role in determining many phenomena in physics and chemistry. An extensive framework of conceptual and computational tools has been developed corresponding to the potential energy landscape approach [1–5], with applications to many-body systems as diverse as metallic clusters, biomolecules, structural glass formers, and coarse-grained models of soft and condensed matter. In all these examples, stationary points of a high-dimensional potential energy function are considered. Due to the non-linear nature of the potential energy as a function of coordinates arising in most real world applications, obtaining the stationary points analytically is not feasible. Hence, one has to rely on numerical methods to obtain the necessary information.

In the present contribution we initiate an extensive numerical analysis of the stationary points of a well-known example, the XY model (without any disorder), for a Hamiltonian defined in terms of the potential energy:

$$H = \frac{1}{N^d} \sum_{j=1}^d \sum_{\mathbf{i}} [1 - \cos(\theta_{\mathbf{i}+\hat{\boldsymbol{\mu}}_j} - \theta_{\mathbf{i}})], \quad (1)$$

where d is the dimension of a lattice, $\hat{\boldsymbol{\mu}}_j$ is the d -dimensional unit vector in the j -th direction, i.e. $\hat{\boldsymbol{\mu}}_1 = (1, 0, \dots, 0)$, $\hat{\boldsymbol{\mu}}_2 = (0, 1, 0, \dots, 0)$, etc., \mathbf{i} stands for the lattice coordinate (i_1, \dots, i_d) , and the sum over \mathbf{i} represents a sum over all i_1, \dots, i_d each running from 1 to N , and each $\theta_{\mathbf{i}} \in (-\pi, \pi]$. Hence d is the dimension of the lattice, and N is the number of sites for each dimension, so the number of θ values required to specify the configuration is N^d . The boundary conditions are given by $\theta_{\mathbf{i}+N\hat{\boldsymbol{\mu}}_j} = (-1)^k \theta_{\mathbf{i}}$ for $1 \leq j \leq d$, where N is the total number of lattice sites in each dimension, with $k = 0$ for periodic boundary conditions (PBC) and $k = 1$ for anti-periodic boundary conditions (APBC). With PBC there is a global degree of freedom leading to a one-parameter family of solutions, as all the equations are unchanged under $\theta_{\mathbf{i}} \rightarrow \theta_{\mathbf{i}} + \alpha, \forall \mathbf{i}$, where α is an arbitrary constant angle, reflecting the fact that the model has global O(2) symmetry. We remove this degree of freedom by fixing one of the variables to zero: $\theta_{(N,N,\dots,N)} = 0$. We have included the factor $1/N^d$ to facilitate comparisons between systems of different sizes. In the present contribution we mainly focus on analysis of local minima and the pathways between them that are mediated by transition states (saddles of index one, with a single negative Hessian eigenvalue [6]).

H appears in many different contexts: first, in statistical physics H is known as the XY Model Hamiltonian and is known to exhibit a Kosterlitz-Thouless transition [7]. It describes a system of N classical planar spin variables, where each spin is coupled to its four nearest neighbors on the lattice. This representation is employed in studies of low temperature superconductivity, superfluid helium, hexatic liquid crystals, and Josephson junction arrays. H also corresponds to the lattice Landau gauge

functional for a compact $U(1)$ lattice gauge theory [8–10], and to the nearest-neighbor Kuramoto model with homogeneous frequency, where the stationary points constitute special configurations in phase space from a non-linear dynamical systems viewpoint [11].

The XY model is among the simplest lattice spin models in which an energy landscape approach based on stationary points of the Hamiltonian in a continuous configuration space is appropriate (unlike, for example, the Ising model whose configuration space is discrete). Nevertheless, we find that the potential energy landscape supports a wide range of interesting features, and proves to be very helpful in analyzing the characteristic structure, dynamics, and thermodynamics.

In Ref. [9, 10] all the stationary points of the one-dimensional XY model were found, including interesting classes, such as stationary wave solutions. In Ref. [9, 12, 13], all the stationary points for the one-dimensional model with anti-periodic boundary conditions were characterized. Solving the stationary equations for the XY model in more than one dimension turned out to be a difficult task and has not been completed to date. In Ref. [9] it was shown how the stationary equations could be viewed as a system of polynomial equations, and the numerical polynomial homotopy continuation (NPHC) method was employed to find all the stationary points for small lattices in two dimensions. This method was subsequently used to study the potential energy landscapes of various other models in statistical mechanics and particle physics [14–23]. In particular, it was employed to study the potential energy landscape of the two-dimensional (2D) XY model [24–26]. In the latter work, along with all the isolated solutions for a small 3×3 lattice, two types of singular solutions were characterized: (1) isolated singular solutions, where the Hessian matrix is singular (these solutions are in fact multiple solutions); and (2) a continuous family of singular solutions. It was shown that one can construct one-, two-, etc. parameter solutions, even after fixing the global $O(2)$ freedom.

In Ref. [25] application of the conjugate gradient method for small N suggested that the number of local minima for the 2D XY model would increase exponentially. One of the important results of the current paper is to verify this conjecture and make it more precise by characterizing the landscapes for larger N values, while improving on the earlier results for the number of minima.

All the above-mentioned minimization methods have a common shortcoming because they cannot deal with even moderately high N (of the order 100 angles). Finding saddles is even harder, and so far the only available results are for 3×3 lattices. In the current paper, we use two more powerful tools to explore the potential energy landscape (PEL) of the 2D XY model in a detailed manner, namely the `OPTIM` package [27], and a GPU-implementation of the overrelaxation method. These approaches can explore the PELs of the 2D XY model with 100 spins and beyond. In the next two Sections, we describe the functionalities of `OPTIM` that we have used in our work and the GPU implementation of the overrelaxation method.

II. METHODS

A. Geometry Optimization

The `OPTIM` program includes a wide variety of geometry optimization tools for characterizing stationary points and the pathways that connect them [27]. The most efficient [28] gradient-only minimization algorithm implemented in `OPTIM` is a modified version of the limited-memory Broyden–Fletcher–Goldfarb–Shanno (LBFGS) algorithm [29, 30]. Both gradient-only and second derivative-based eigenvector-following [31, 32] and hybrid eigenvector-following algorithms [33, 34] are available for single- and double-ended [35] transition state searches. Stationary points with any specified Hessian index can also be located [36].

We used `OPTIM` to sample minima and transition states for the 2D XY model with both PBC and APBC, using exclusively single-ended search algorithms. In particular, we refined 500,000 random initial guesses for all lattice sizes up to $N = 10$, i.e., a total of 100 spins. In each case there also exist degenerate stationary points related by symmetry operations of the Hamiltonian with $\theta_{\mathbf{i}} \rightarrow -\theta_{\mathbf{i}}$ for all N^d angular variables as well as $\theta_{\mathbf{i}} \rightarrow \theta_{\mathbf{i}} \pm (\pi, \pi, \dots, \pi)$.

B. GPU Implementation of Overrelaxation

Another approach that we applied to obtain as many minima as possible employed the (over)relaxation algorithm exploiting graphics processing units (GPUs), which offer a high level of parallelism and thus enabled us to generate large samples within a practical amount of computer time. The idea of the relaxation algorithm is to sweep over the lattice while optimizing the Hamiltonian locally on each lattice site. Our implementation is based on the *www.cuLGT.com* code [37].

In practice we employed four cards of the NVIDIA Tesla C2070 and launched 1024 thread blocks (i.e. samples) per GPU. We kept the grid size as 1024 blocks per GPU fixed and then cycled over $2^{17} = 131072$ iterations, resulting in around 0.134 billion samples per lattice size. We set the overrelaxation parameter to 1.0, i.e. standard relaxation, to increase the chance of finding minima with small basins of attraction. For each sample we stored the value of the minimum to which the relaxation algorithm converged along with the N^d corresponding θ -coordinates, and subsequently sorted these values via bitonic sort [38], again accelerated by the GPU. As a stopping criterion we required the largest gradient over all lattice sites to be smaller than 10^{-12} (reduced units). The whole simulation was performed in double precision to reduce numerical inaccuracies.

III. RESULTS

We first point out that the global minimum of this model, as it does not have any disorder, is well known: for the APBC case, $\theta_i = 0$ or π for all N^d angular variables are the two global minima of the model at which $H = 0$. Similarly, for the PBC case, because we have fixed the $\mathcal{O}(2)$ symmetry, the unique global minimum corresponds to $\theta_i = 0$ for all angles, again with $H = 0$.

A. Number of Minima and Transition States

In Table I we summarize the number of minima and transition states located for each N . Here, in addition to finding minima and transition states for larger lattices, we have also improved our previous results for the number of minima from Ref. [25] at smaller N with the help of the more powerful algorithms. Saddles of index one were only obtained from the OPTIM runs. Since the 2D XY model possesses a number of discrete symmetries, as discussed in [25], we also tabulate the number of distinct minima and transition states in the table, i.e. solutions unrelated by symmetries of the Hamiltonian. In contrast to $N \leq 8$, for larger N our samples will be substantially incomplete, even though we have found around 5.5 million minima for the $N = 16$ case. As expected from symmetries of the Hamiltonian [25], for each N with PBC the global minimum is unique, the next minimum is 4-fold degenerate, then $N^2/2$ -fold degenerate (if N is even), then $2N^2$, $4N^2$, $2N^2, \dots, N^2/2$ (if N is even), and the highest energy minimum is 4-fold degenerate. For the APBC case the global minimum is 2-fold degenerate, and all other minima are at least N^2 degenerate.

The number of minima and transition states located as a function of N are plotted in Figure 1. The plot clearly shows that the total number of minima (including degeneracies), the number of distinct minima, the total number transition states, and the number of distinct transition states, all increase roughly exponentially with increasing N , as expected [36, 39]. We also observe abrupt jumps at $N = 7$ and 9 for the PBC case, and at $N = 6$ for the APBC cases in this plot, though the precise reason of this behavior is not clear. It is possible that the jumps are caused by sampling issues, but there could be a more subtle explanation; for example, certain lattices for particular values of N may restrict the possible classes of minima.

For both APBC and PBC the energies of the local minima shift towards lower energy as N increases, tending to accumulate near the global minima. This behavior has previously been observed in the 1D XY model with PBC [25]. In this case, the potential energy distribution of the minima has a spike for the global minimum at $H = 0$ and a two-fold degeneracy for other minima in $H \in (0, 1]$. Since every minimum in the ordered 1D XY model has a higher-dimensional analogue with the same energy [25],

it is not surprising that the 2D PBC case exhibits similar behavior. Straightforward construction of higher-dimensional saddles from lower-dimensional ones is not possible in APBC, so it is interesting to see the 2D APBC XY model behaving differently from the 1D APBC XY model, but similar to the 2D PBC case. In future work, we also intend to *certify* these solutions using techniques based on Smale’s α -theorem [41].

B. Disconnectivity Graphs

Disconnectivity graphs have provided a particularly useful tool for visualizing potential and free energy landscapes [40, 42–44] in systems ranging from atomic and molecular clusters to soft and condensed matter and biomolecules [1–3]. In particular, this construction enables the lowest potential or free energy barriers to be faithfully represented, and can help us to understand how observable properties emerge from features of the landscape [45].

To produce a disconnectivity graph we require a kinetic transition network [45–47], which can be defined by a database of local minima and the transition states that connect them [40]. We then choose a regular energy spacing, ΔV , and determine how the minima are partitioned into subsets (superbasins [40]) at energies $V_0, V_0 + \Delta V, V_0 + 2\Delta V, \dots$. These subsets consist of minima that can interconvert via index one saddles that lie below the energy threshold. For a high enough threshold all the minima can interconvert and there is just one superbasin, unless there are infinitely high barriers. As the threshold energy decreases the superbasins split apart, and this splitting is represented in the disconnectivity graph by lines connecting subgroups to parent superbasins at the threshold energy above. The superbasins terminate at the energies of individual local minima, which may be grouped together for degenerate states related by symmetry operations of the Hamiltonian.

The significance of the disconnectivity graph construction stems primarily from the insight it provides into the global thermodynamics and kinetics of the system in question. For example, if the landscape supports alternative morphologies separated by a high barrier then we anticipate a separation of relaxation time scales and associated features in the heat capacity [1–3, 45]. Several limiting cases have been identified for the organization of the landscape, distinguishing good ‘structure seeking’ systems, which exhibit efficient relaxation to the global minimum, from models with glassy characteristics [42]. These visualisations have much in common with the ‘energy lid’ and ‘energy threshold’ approaches of Sibani, Schön, and coworkers [48–52].

In the current contribution we have characterized both minima and transition states, which enables us to construct the first disconnectivity graphs for XY models (Figures 2 and 3). These graphs all correspond to the structure expected for efficient relaxation to the global minimum over a wide range of

temperature (or total energy), namely the ‘palm tree’ motif [42]. Locating low-lying minima for these 2D XY models should therefore be relatively straightforward: relaxation following the intrinsic dynamics of the system should lead to the global minimum for temperatures of physical interest. This is the pattern that we associate with good structure-seeking systems [2, 4, 42, 45], including ‘magic number’ clusters such as buckminsterfullerene, self-assembling mesoscopic structures such as virus capsids, crystallisation, and proteins that fold into functional native states on in vivo time scales.

C. Energy Differences

Experimentally, it is not the absolute value of the energy but rather energy differences that are measured. For the 2D XY model with no disorder, we can in principle study $dE_{k,l}^i = E_k^i - E_l^i$, where E_k^i is the energy of the k -th index i saddle in order of increasing energy. For the 2D XY model, the global minimum has energy $E_0^0 \equiv E_0 = 0$ yielding $dE_{k,0}^0 = E_k^0$. The sequential energy differences $dE_{k+1,k}^i$ are particularly interesting, since all other energy differences can be obtained from them. We plot N vs $dE_{k+1,k}^0$ in Figure 4 and N vs $dE_{k+1,k}^1$ in Figure 5. We find that that the sequential energy differences decay towards zero as N increases.

This observation is similar to results for the 1D XY model with PBC. There, in the continuum limit, the energies of the local minima are distributed continuously over the range $[0, 1]$. However, there is a spike in the density of minima at $E_0 = 0$, while other energy values are two-fold degenerate. For small N , it appears as if $dE_{k,0}^0$ is decaying towards zero. However, as N becomes large enough, $dE_{k,0}^0$ eventually starts to fill in $[0, 1]$, with a maximum in the density of minima that approaches the global minimum [25]. In fact, it is the energy difference between sequential minima, $dE_{k+1,k}^0$, that decays towards zero. For every saddle in 1D with PBC, we can build a higher dimensional analogue that has the same energy [25]. Hence, the energy spectrum of the 2D XY model with PBC and no disorder contains at least one copy of the 1D XY model with PBC.

$dE_{k,0}^0$ has been studied in reference [25], where it was found to decay to zero for the smaller lattice sizes. The results in Figures 4 and 5, coupled to the previous 1D PBC observations, suggest that that $dE_{k+1,k}^0$ tends to zero, while $dE_{k,0}^0$ fills up a continuous spectrum spanning at least $[0, 1]$. The 2D XY model with APBC seems to follow a similar pattern to the PBC case.

D. Barrier Heights

The average uphill/downhill barrier between minima and transition states can be defined [53] as

$$\langle \Delta \rangle = \langle E_{\text{ts}} \rangle - \sum_{\gamma} n_{\text{ts}}^{\gamma} E_{\text{min}}^{\gamma} / 2n_{\text{ts}}$$

where E_{\min}^{γ} is the energy of the minimum γ and n_{ts}^{γ} is the number of transition states connected to that minimum. The naive uphill/downhill barrier is given by

$$\langle \Lambda \rangle = \langle E_{\text{ts}} - E_{\min} \rangle.$$

As noted in [53], the average over minima in the second term of $\langle \Delta \rangle$ is usually weighted towards the lower energy minima, since they are connected to more transition states. This organisation makes $\langle \Delta \rangle$ larger than $\langle \Lambda \rangle$, as we see in the plots of the average barriers in Figures 6. In these plots, only distinct non-degenerate lowest-energy rearrangements were considered in the averages.

IV. CONCLUSIONS

The potential energy landscape has been examined for the two-dimensional XY model (with no disorder) with both periodic and anti-periodic boundary conditions. Lattices with up to $N = 10$ lattice sites in each direction, i.e. 100 spins, were considered, focusing on the potential energy distribution of minima and the transition states (saddles of index one) that connect them. As expected [36, 39], the number of stationary points increases roughly exponentially with the number of degrees of freedom. Knowledge of the pathways that connect the local minima enables us to construct the first disconnectivity graphs for the XY model, and hence visualize the potential energy landscape. These graphs reveal that the landscape is funnelled in each case, with a well-defined global minimum, and small downhill barriers connecting this structure to the higher-energy configurations. Hence all of these 2D XY landscapes belong to the class of systems identified as good ‘structure seekers’, which includes ‘magic number’ atomic and molecular clusters, naturally occurring proteins, and self-assembling mesoscopic systems, including crystals [2, 4, 42, 45]. Minimization from random starting points confirms that the global minimum is readily located in each case; the funnelled organisation of the landscape is reinforced by the existence of relatively large basins of attraction for the global minima compared to the higher energy minima, and this effect grows with increasing lattice size.

Although the samples of stationary points are not exhaustive for the larger lattice sizes, we can draw some further general conclusions. First, for a given lattice size, N , there are more minima for antiperiodic boundaries than for periodic boundary conditions. Second, as N increases the energy range spanned by the local minima increases, as one might expect from extensivity of the energy. This effect is also visible in the disconnectivity graphs. However, the probability distribution for the energy of the local minima tends to shift towards the global minimum for larger lattice sizes.

The trends we have identified have far-reaching implications for the thermodynamics and global kinetics of the 2D XY model, which we will investigate in future work. Given the wide-ranging applications

of this model, which include superconductivity, superfluidity, liquid crystals, Josephson junctions, and the fundamental importance of this Hamiltonian in lattice gauge theory [8–10], the energy landscape perspective may provide new insight into a variety of different research fields.

DM was supported by the U.S. Department of Energy under contract no. DE-FG02-85ER40237 and DARPA Young Faculty Award. CH acknowledges support from Science and Technology Facilities Council and the Cambridge Home and European Scholarship Scheme. MS acknowledges support by the Research Executive Agency (REA) of the European Union under Grant Agreement PITN-GA-2009-238353 (ITN STRONGnet). DJW gratefully acknowledges support from the EPSRC and the ERC.

-
- [1] D. J. Wales. *Energy Landscapes : Applications to Clusters, Biomolecules and Glasses (Cambridge Molecular Science)*. Cambridge University Press, January 2004.
 - [2] D. J. Wales. *Phil. Trans. Roy. Soc. A*, **363** 357–377 (2005).
 - [3] D. J. Wales and T. V. Bogdan. *J. Phys. Chem. B*, **110** 20765–20776 (2006).
 - [4] D. J. Wales. *Phil. Trans. Roy. Soc. A*, **370** 2877–2899 (2012).
 - [5] M. Kastner. *Rev. Mod. Phys.*, **80** (1) 167–187 (2008).
 - [6] J. N. Murrell and K. J. Laidler. *Trans. Faraday. Soc.*, **64** 371–377 (1968).
 - [7] J. M. Kosterlitz and D. J. Thouless. *J. Phys. C: Solid State Physics*, **6** 1181 (1973).
 - [8] A. Maas. *Phys. Rept.*, **524** 203 (2013).
 - [9] D. Mehta. *Ph.D. Thesis, The Uni. of Adelaide, Australasian Digital Theses Program* (2009).
 - [10] D. Mehta and M. Kastner. *Annals Phys.*, **326** 1425 (2011).
 - [11] J. A. Acebrón, L. L. Bonilla, C. J. P. Vicente, F. Ritort and R. Spigler. *Rev. Mod. Phys.*, **77** 137 (2005).
 - [12] L. von Smekal, D. Mehta, A. Sternbeck and A. G. Williams. *PoS, LAT2007* **382** (2007).
 - [13] L. von Smekal, A. Jorkowski, D. Mehta and A. Sternbeck. *PoS, CONFINEMENT8* **048** (2008).
 - [14] D. Mehta. *Phys. Rev. E*, **84** 025702 (2011).
 - [15] D. Mehta. *Adv. High Energy Phys.*, **2011** 263937 (2011).
 - [16] M. Maniatis and D. Mehta. *Eur. Phys. J. Plus*, **127** 91 (2012).
 - [17] M. Kastner and D. Mehta. *Phys. Rev. Lett.*, **107** 160602 (2011).
 - [18] D. Mehta, Y.-H. He, and J. D. Hauenstein. *JHEP*, **1207** 018 (2012).
 - [19] D. Mehta, J. D. Hauenstein, and M. Kastner. *Phys. Rev. E*, **85** 061103 (2012).
 - [20] D. Mehta, D. A. Stariolo, and M. Kastner. *Phys. Rev. E* **87**, 052143 (2013).
 - [21] B. Greene, D. Kagan, A. Masoumi, D. Mehta, E. J. Weinberg and X. Xiao. *Phys. Rev. D* **88** 026005 (2013).

- [22] D. Martinez-Pedrerera, D. Mehta, M. Rummel and A. Westphal. *JHEP* **1306**, 110 (2013).
- [23] Y.-H. He, D. Mehta, M. Niemerg, M. Rummel and A. Valeanu. *JHEP* **1307**, 050 (2013).
- [24] D. Mehta, A. Sternbeck, L. von Smekal, and A. G. Williams. *PoS, QCD-TNT09* 025 (2009).
- [25] C. Hughes, D. Mehta, and J. I. Skullerud. *Annals Phys.* **331**, 188 (2013).
- [26] R. Nerattini, M. Kastner, D. Mehta and L. Casetti, *Phys. Rev. E*, **87** 032140 (2013).
- [27] D. J. Wales. OPTIM: A program for optimising geometries and calculating pathways.
<http://www-wales.ch.cam.ac.uk/software.html>
- [28] D. Asenjo, J. D. Stevenson, D. J. Wales, and D. Frenkel. *J. Phys. Chem. B*, **000** 0000 (2013).
- [29] J. Nocedal. *Mathematics of Computation*, **35** 773 (1980).
- [30] D. Liu and J. Nocedal. *Math. Prog.*, **45** 503 (1989).
- [31] D. J. Wales. *J. Chem. Soc. Faraday Trans.*, **88** 653 (1992).
- [32] D. J. Wales. *J. Chem. Soc. Faraday Trans.*, **89** 1305 (1993).
- [33] L. J. Munro and D. J. Wales. *Phys. Rev. B*, **59** 3969 (1999).
- [34] Y. Kumeda, L. J. Munro, and D. J. Wales. *Chem. Phys. Lett.*, **341** 185 (2001).
- [35] S. A. Trygubenko and D. J. Wales. *J. Chem. Phys.*, **120** 2082 (2004).
- [36] D. J. Wales and J. P. K. Doye. *J. Chem. Phys.*, **119** 12409 (2003).
- [37] M. Schröck and H. Vogt. *Comp. Phys. Commun.*, **184** 1907 (2013).
- [38] K. E. Batcher. *Proc. AFIPS Spring Joint Comput. Conf.*, **32** 307 (1968).
- [39] F. H. Stillinger and T. A. Weber. *Science*, **225** 983 (1984).
- [40] O. M. Becker and M. Karplus. *J. Chem. Phys.*, **106** 1495 (1997).
- [41] D. Mehta, J. D. Hauenstein, and D. J. Wales. *J. Chem. Phys.*, **138**, 171101 (2013).
- [42] D. J. Wales, M. A. Miller, and T. R Walsh. *Nature*, **394** 758 (1998).
- [43] S. V. Krivov and M. Karplus. *J. Chem. Phys.*, **117** 10894 (2002).
- [44] D. A. Evans and D. J. Wales. *J. Chem. Phys.*, **118** 3891 (2003).
- [45] D. J. Wales. *Curr. Op. Struct. Biol.*, **20** 3 (2010).
- [46] F. Noé and S. Fischer. *Curr. Op. Struct. Biol.*, **18** 154 (2008).
- [47] D. Prada-Gracia, J. Gómez-Gardenes, P. Echenique, and F. Fernando. *PLoS Comput. Biol.*, **5** 1 (2009).
- [48] P. Sibani, J. C. Schön, P. Salamon and J. -O. Andersson, *Europhys. Lett.* **22** 479 (1993).
- [49] P. Sibani and P. Schriver, *Phys. Rev. B* **49** 6667 (1994).
- [50] J. C. Schön, *Ber. Bunsenges. Phys. Chem.* **100** 1388 (1996).
- [51] J. C. Schön, H. Putz and M. Jansen, *J. Phys. Condensed Matter.* **8** 143 (1996).
- [52] J. C. Schön, *J. Phys. Chem. A* **106** 10886 (2002).
- [53] D. J. Wales and J. P. K. Doye. *J. Chem. Phys.*, **116** 3777 (2002).

TABLES

N	3	4	5	6	7	8	9	10	12	14	16
minima (APBC)	2	66	202	146	1570	7170	24626	99207	849329	2826736	5606875
distinct minima (APBC)	1	2	2	2	4	13	20	49	298	1671	10876
saddles of index 1 (APBC)	18	288	850	3864	13890	27456	51234	52572			
distinct saddles of index 1 (APBC)	1	2	3	8	15	73	201	615			
minima (PBC)	1	1	9	27	9	681	44000	13918	111699	704547	2593377
distinct minima (PBC)	1	1	3	4	3	8	14	44	257	2266	23352
saddles of index 1 (PBC)	9	16	71	234	277	2540	3587	3854			
distinct saddles of index 1 (PBC)	1	1	3	5	3	17	30	115			

Table I: The number of minima and saddles of index one located for different lattice sizes $N \times N$, with both PBC and APBC.

FIGURES

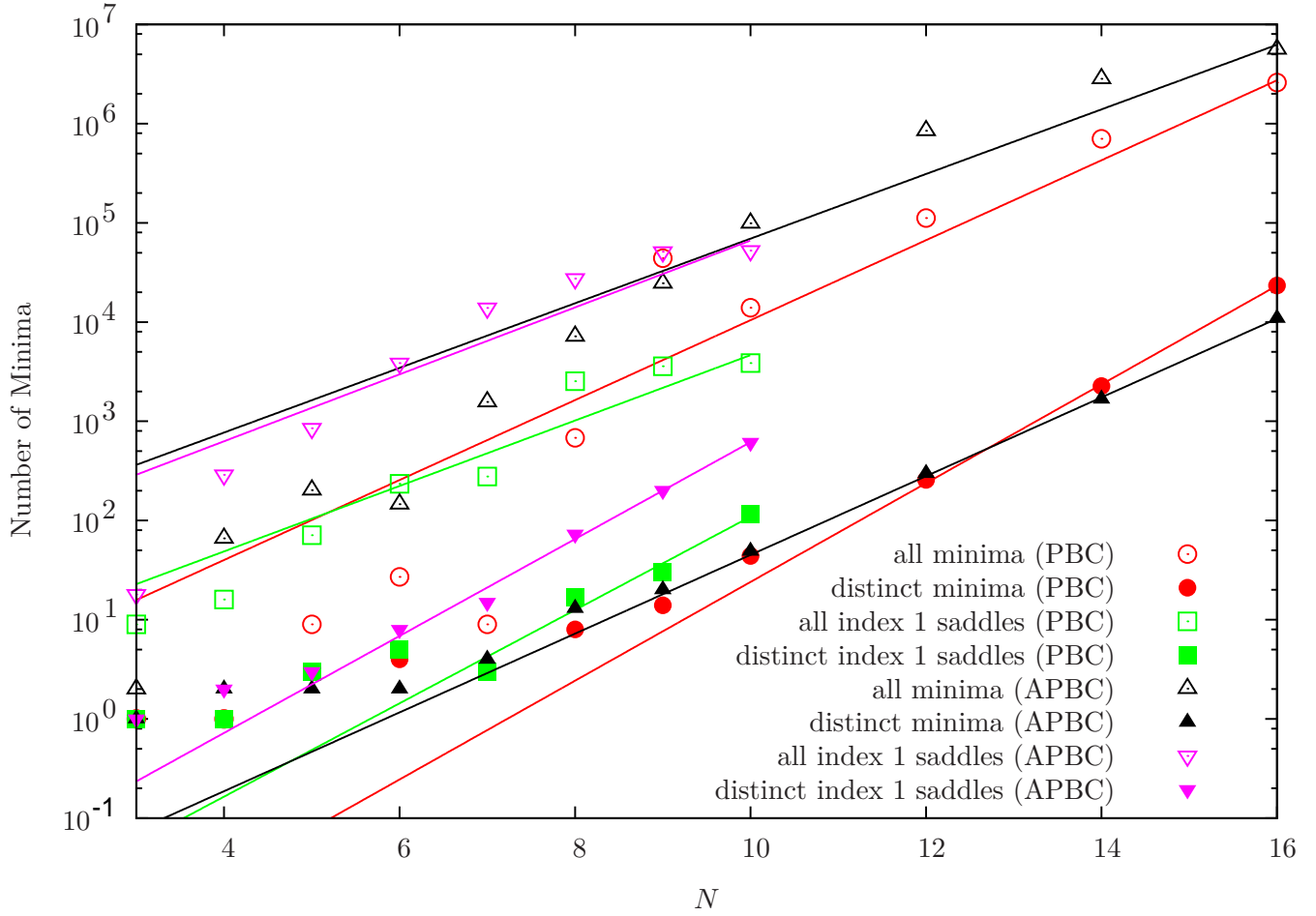


Figure 1: Number of minima as a function of the number of lattice sites, N , for each dimension. The straight lines are the corresponding best fits for the data-points, i.e. the number of distinct minima and the total number of minima including degeneracies increases roughly exponentially with increasing N .

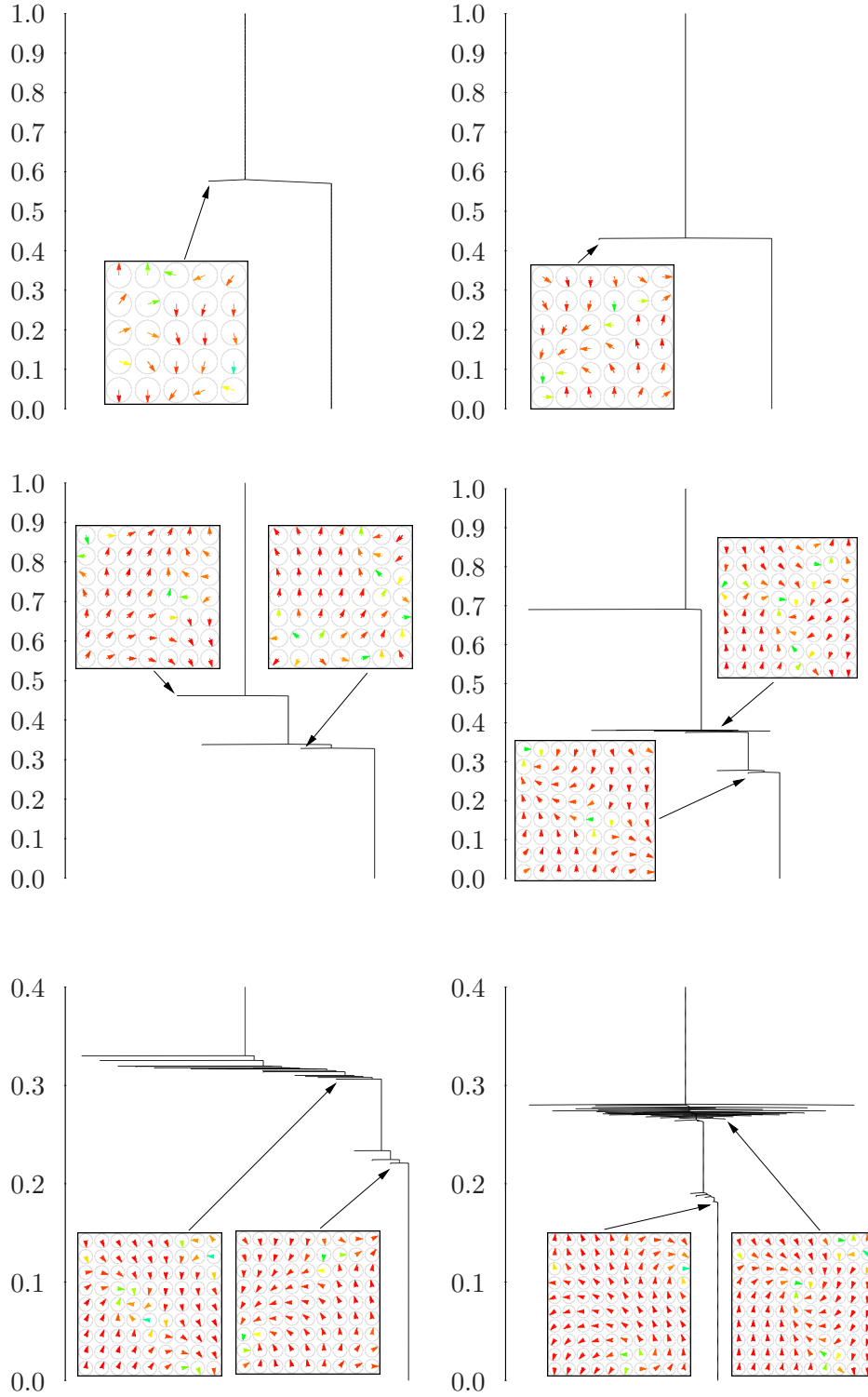


Figure 2: Disconnectivity graphs for the 5×5 , 6×6 , 7×7 , 8×8 , 9×9 and 10×10 APBC lattices.

Each of the two insets represents an example minimum for the corresponding $N \times N$ lattice. Each arrow in these insets represents the corresponding value of $\theta_{\mathbf{i}}$ at the lattice-site \mathbf{i} . At each lattice site \mathbf{i} , we compute the local energy $\sum_{j=1}^d (1 - \cos(\theta_{\mathbf{i}+\hat{\mu}_j} - \theta_{\mathbf{i}}))$, which is in the range $[0, 4]$. We colour the arrows red-orange-yellow-green-blue-indigo-violet from the lowest to highest local energies.

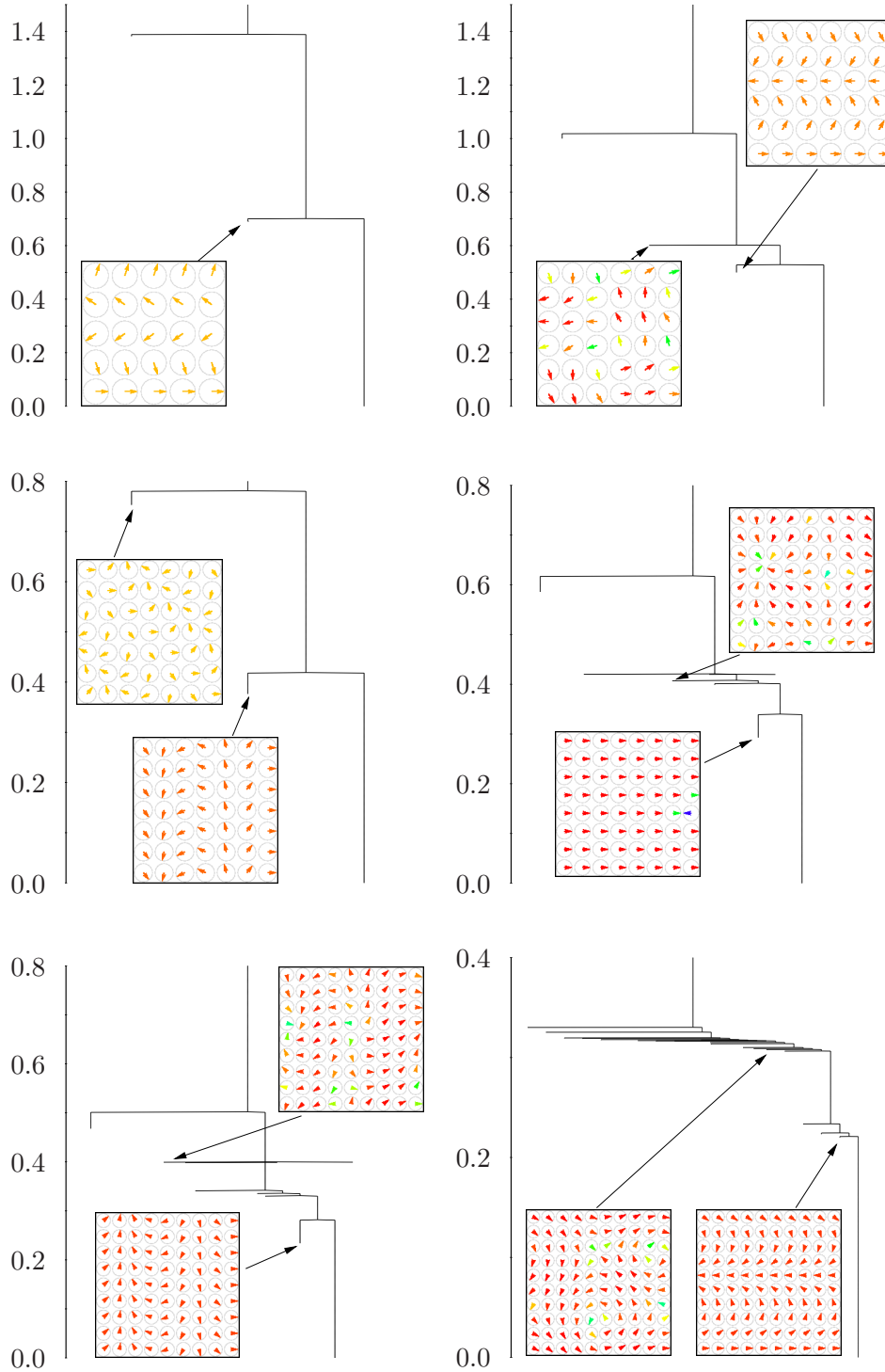


Figure 3: Disconnectivity graphs for 5×5 , 6×6 , 7×7 , 8×8 , 9×9 and 10×10 PBC lattices. Each of the two insets represents an example minimum for the corresponding $N \times N$ lattice. Each arrow in these insets represents the corresponding value of $\theta_{\mathbf{i}}$ at the lattice-site \mathbf{i} . At each lattice site \mathbf{i} , we compute the local energy $\sum_{j=1}^d (1 - \cos(\theta_{\mathbf{i}+\hat{\mu}_j} - \theta_{\mathbf{i}}))$, which is in the range $[0, 4]$. We colour the arrows red-orange-yellow-green-blue-indigo-violet from the lowest to highest local energies.

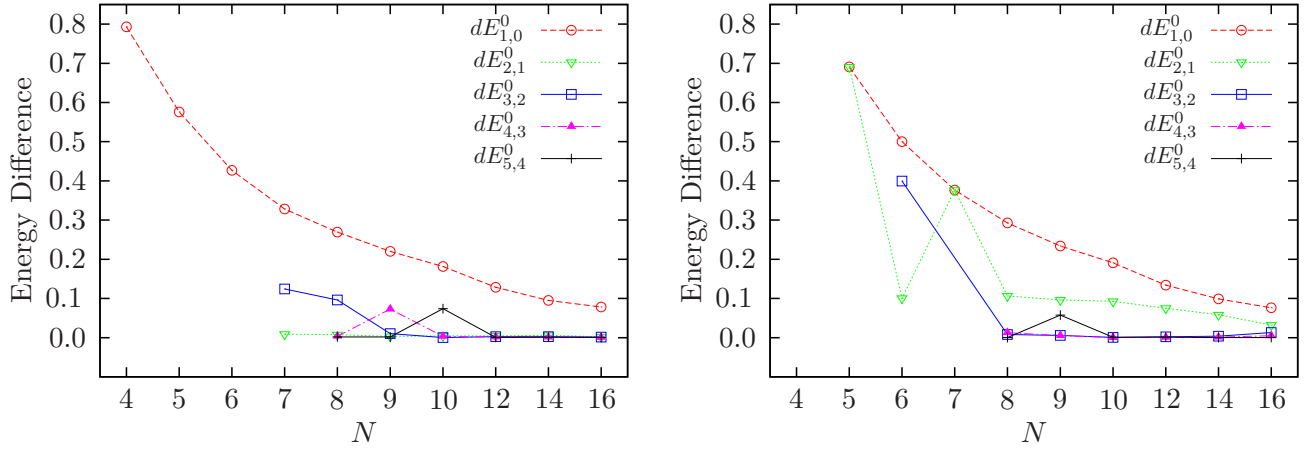


Figure 4: Sequential energy differences between minima when ranked energetically for APBC (left) and PBC (right) as a function of lattice dimension N . $dE_{k+1,k}^0$ is the energy difference between minima $k+1$ and k when arranged in increasing order from $k=0$.

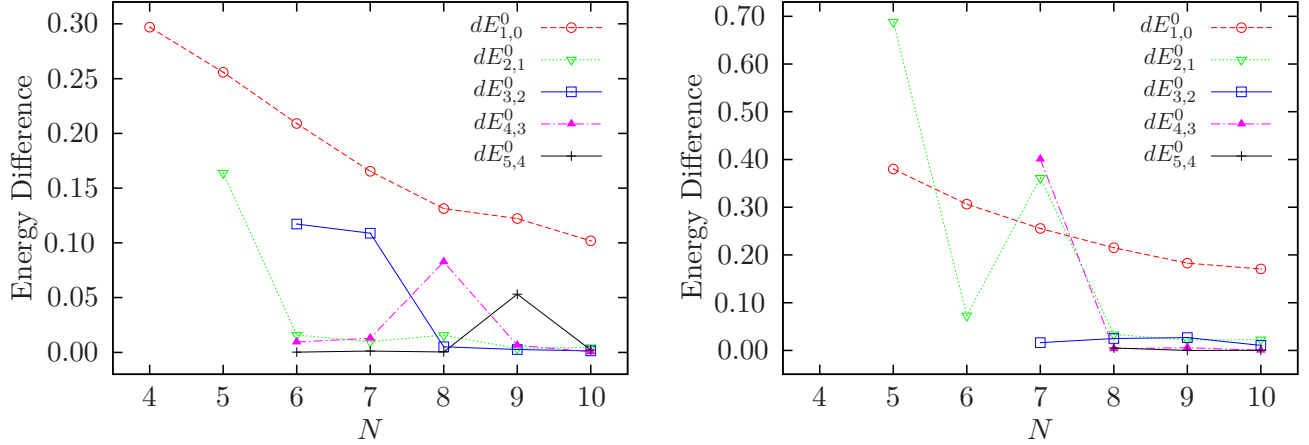


Figure 5: Sequential energy differences between transition states $k+1$ and k when ranked energetically for APBC (left) and PBC (right) as a function of lattice dimension N . $dE_{k+1,k}^1$ is the energy difference between transition states $k+1$ and k when arranged in increasing order from $k=0$.

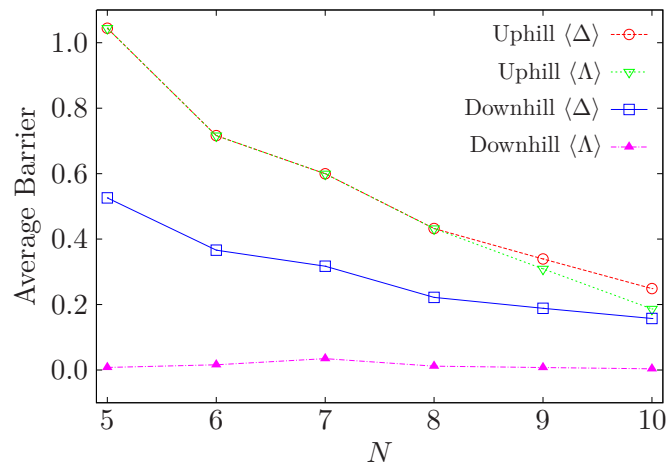
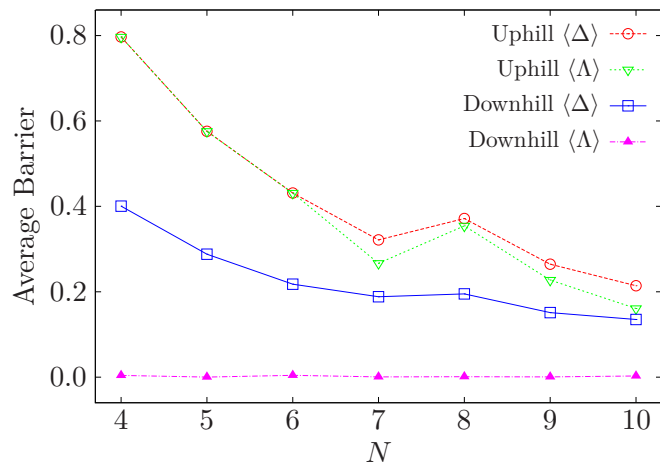


Figure 6: Average value of barrier from $\langle \Delta \rangle$ and $\langle \Lambda \rangle$ for APBC and PBC.